Numerical Study of flow-through the perforations for angle perforation 180° and 90° in horizontal wellbore

Mohammed A. Mustafa[1], Qais A. Rishak[2], Mohammed A. Abdulwahid [3]
{Pgs2338@uobasrah.edu.iq[1], qais.rashck@uobasrah.edu.iq[2], mohw2016@stu.edu.iq [3]}

The University of Basrah. Mechanical Engineering Department [1]
The University of Basrah. Materials Engineering Department[2]
Southern Technical University, Basrah. Thermal Mechanical Engineering Department [3]

Abstract. A numerical study is carried out on the perforation pipes with phase angles of 180° and 90° in a horizontal wellbore. To understand the effect of the above two-phase angles on the flow inside the wellbore, the CFD simulation of computational fluid dynamics is used. ANSYS FLUENT's simulation of the flow in the well has been used to calculate the pressure drop, friction factor, wall shear stress, productivity index, etc. The standard $(k-\varepsilon)$ model has been used to predict the turbulent behavior of radial flow. The conclusion showed that the overall pressure drop increase as the flow rate ratio increase which leads to an increase in the radial flow through the perforations, thereby keeping the axial flow through the pipe constant. Therefore, the percentage error of the total pressure drops for the phasing of the 180° and 90° perforations in test 5 is about 5.4 %. In addition, the main flow increases when the flow through the perforation increases, and this leads to an increase in the average of wall shear stress.

Keywords: CFD, Perforation, Horizontal Well, Pressure Drop, Productivity Index

1 Introduction

Horizontal wells have become commonplace in the petroleum business. Due to the pressure drop in the well, the productivity of horizontal wells will be limited. During flow from the horizontal end (toe) to the end (heel) horizontal, the pressure drop in the well is imminent. Therefore, the pressure drop in the well is important to compare to the storage tank, pulling the tank along the length of the good changes, therefore production along the good length will also change. Locke [1] proposed a new theoretical model to predict horizontal good productivity, by building a very right simulation model, precise limit element methods were used to simulate operations. These analyses confirmed previous results that the angle of the perforations 90 degrees is better than the test angles 0, 120, and 180 degrees, but it produces greater amounts of inflow through the perforations. Subsequently, others [2-5] continued their research, and they proposed different coupling models of well flow and perforation into the reservoir. However, in some case studies, only the friction component is observed to study the pressure drops across the wellbore.The most probable case: acceleration was considered when studying pressure drop, and other effects such as flow, mixing, etc. were ignored.

The first study of fluid mixing between internal and main flow was raised flow provided by Su and Gudmundsson [6] studied the effect of the overall pressure drop in a perforated horizontal wellbore with fluid flow through the perforation where two fluids are mixed at junctions. Using the experimental parameters on a perforated pipe has an inner diameter of 22.2 mm, length of 2 m, and a Perforation diameter of 3 mm, a perforation density of 12 spf, and a 60° phasing. The results explain that the friction wall drop of pressure is about 80%, the flow mixing pressure drop (including perforation roughness) is about 15% and the acceleration pressure drop is about 5% of the overall pressure drop. Novy [7] studied the effect of friction losses on the pressure drop inside the horizontal wellbore, flow throughout the system is single phase and steady. The results showed that the decrease in pressure is important for shrinkage (the pressure difference

IMDC-IST 2021, September 07-09, Sakarya, Turkey

DOI 10.4108/eai.7-9-2021.2314933

between the reservoir and the wellbore), so the pressure can approximately equal the pressure in the reservoir. Asheim et al. [8] suggested a model for fluid resistance for a theoretically horizontal perforated well. This model has one or two perforations with a diameter of 12.7 mm and length are 200 mm and it is made from the experimental group of test section pipe (50, 100, and 150 mm). The results showed that the proposed fluid flow resistance model gives excellent compatibility compared to the experimental results. Campos et al. [9] a mathematical model is developed based on conservation equations for mass and momentum. The experimental results showed excellent compatibility with the proposed fluid flow resistance model. From this work, the determined the effects of an acceleration and friction pressure drop on the total oil well productivity index. Fayal and Lakhdar [10] proposed a research model for the established pressure drop caused by friction and acceleration in a horizontal well with constant and single-phase flow. ANSYS FLUENT and disordered (k-ε) models were used to determine the entrance length. The result showed that the pressure drop due to acceleration was significant and equal to 30% of the total pressure and friction pressure drop due to perforation was neglected.
Abdulwahid et al. [11] provided a numerical simulation model of a pipeline flow with two perforations, one on the upper and one on the lower surface. Using ANSYS to analyse the overall pressure drops, the static pressure, and the average wall shear stress distribution of a horizontal well with a diameter of 22 mm and a length of 1 m. There are two perforations with perforation diameters of 0.006 m and 0.003 m. It is used the RNG (k-ε) model in the plane of symmetry model. Their results showed that the total pressure drop increases as increasing the axial velocity and vice versa.

The main objective of this paper is to analyse numerically the effect of pressure drop in perforation of a horizontal wellbore. Which is including the wall friction, mixing, and acceleration, that contribute to the total pressure drop in a perforated pipe. As well as study the effect of the friction factor, productivity index, and the effect of the change in the quantities of flow through the perforations and the axial flow in perforation a horizontal well of the angle of 180°, and 90°. It is noticed that the productivity index of the angle perforation 90° is higher than the perforation angle of 180°. As a result of increasing the amount of flow through the perforations for an angle of 90° greater than the angle of 180°.

2 Numerical Simulations

The rapid advancement of computer technologies and software enables the solution of theoretical simulations for complex applications. This paper investigates a Numerical analysis of a single-phase flow through a horizontal wellbore. The mathematical simulation with a 3D model with turbulent flow in the horizontal wellbore is performed. Using CFD ANSYS FLUENT. The horizontal wellbore simulation is carried out using the conservation law (mass, momentum) in conjunction with the perturbation (k-ε) model.

The numerical analysis of the fluid flow field is solved using ANSYS FLUENT. The ANSYS FLUENT is used to solve the numerical analysis of the fluid flow field. The cell-vertex finite volume method is used by ANSYS FLUENT solvers. A fixed number of the control volumes are created from the fluid region.

3 Description of the Models

In the current study, the numerical analysis is made with ANSYS FLUENT. It is used the stander k-ε model. The physical models are developed in the two PVC pipes with a perforations surface roughness of 0.03mm. The first pipe is 18 perforations divided into two lines with 180^{o} perforation phasing. Each line has 9 perforations. The second pipe has 20 perforations divided into four lines with perforation phasing 90^{o} each line has 4 perforations. The length of the pipe that drawing in ANSYS is 2 m, 44 mm inner diameter, and 4 mm perforation diameter. The pipe is divided into three sections. The first section in length 0.250 m is blank, and the second

is part of the pipe of 1 m of the perforation phasing 180 ° and 90°. The third section in length 0.75 m is blank, As shown in Fig.1 the model of the perforation pipe.

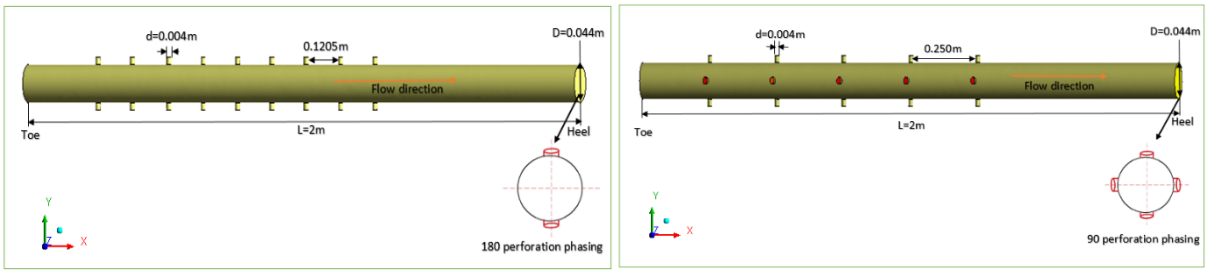

Fig.1. The physical model for 180° and 90° perforation phasing.

4 Assumptions and Simulation Parameters

The water density of 1000 kg/m^3, the dynamic viscosity of 0.00103 kg/ms, and water at 25° of the water (isothermal) are applied in our work. It is analysed the pressure, friction, and productivity index.

The present work is based on single-phase, turbulent flow, steady-state flow, Newtonian fluid, incompressible flow, and no heat transfer related the system to surroundings.

4.1 Boundary Condition

The solving of the management equations system of a CFD can only be used if the solution meets certain boundary constraints. As a result, we must supply boundary conditions to a CFD solver. Boundary inputs can be utilized to convert a CFD model counterpart to a real situation in a variety of ways. In ANSYS fluent, there are numerous techniques for describing fluid limitations.

Inlet B.C

The inlet boundary condition is used where the flow is directed mainly to the domain, the normal velocity is specified directly at the inlet. This process occurs during the Fluent-Solver process.Axial flow through the main horizontal wellbore

$$Q = U_1 * A \tag{1}$$

Q = axial flow rate of the main pipe m^3 /s

Radial flow through a perforation in the pipe

$$q = \mathrm{n}\frac{\pi}{4}\mathrm{d}^2\,\mathrm{U}_2 \tag{2}$$

q =inflow through perforation flow rate m^3/s

Tests are performed at different flow rates of the axial flow through the main pipe and radial flow through the perforations in all these tests are shown in Table 1. In the case of turbulent flow, the flow rates are selected based on the values of Reynolds number, which is greater than 4000.

Table 1. Details of the flow.

Flow Test	Axial flow (lit/min)	Radial flow rate (lit/min)
Test 1	40	**0 – 80**
Test 2	60	**0 – 80**
Test 3	80	**0 – 80**
Test 4	120	**0 – 80**
Test 5	160	**0 – 80**

Outlet B.C

The outlet boundary condition can be used where the flow is known to be out of the domain. In the present cases, the present relative static pressure (Ps) at the output is zero. The inlet pressure required to sustain the specified flow will be determined using ANSYS fluent.

$$P=Ps=0 \tag{3}$$

4.2 Governing Equations

Pressure variations owing to friction losses in the horizontal pipe and perforations, perforation roughness, mixing effect, acceleration, and changes in the volume of flow between the perforations and the main pipe all affect fluid flow in a horizontal perforated wellbore. Therefore, the two main equations for fluid flow (the equations for mass and momentum) are required to properly describe these physical changes [12].

Conservation of mass

The equation for conservation of mass is described as follows:

$$\rho \frac{\partial}{\partial x_i}(u_i) = 0 \tag{4}$$

Conservation of Momentum

In Cartesian coordinates, the momentum conservation equation is represented as follows:

$$\frac{\partial}{\partial t}(\rho u_i) + u_j \frac{\partial(\rho u_i)}{\partial x_j} = -\frac{\partial P}{\partial x_i} + \frac{\partial}{\partial x_j}(\tau_{ji}) + F_i \tag{5}$$

The strain rate tensor can be used to rewrite the viscous stress tensor.

$$\tau_{ji} = \mu\left(\frac{\partial u_j}{\partial x_i} + \frac{\partial u_i}{\partial x_j}\right) = 2\mu S_{ji} \tag{6}$$

Substitute Eq. (5) into Eq. (4), This produces;

$$\rho \frac{\partial}{\partial x_j}(u_i u_j) = -\frac{\partial P}{\partial x_i} + \frac{\partial}{\partial x_j}(2\mu S_{ji}) + F_i \tag{7}$$

In turbulent flow, the instantaneous quantities can be broken up into mean and fluctuating components.

$$u_i = \bar{u}_i + u_i' \ . \ u_j = \bar{u}_j + u_j' \ . P = \bar{P} + P'$$
$$S_{ji} = \overline{S_n} + S_{ji}' \tag{8}$$

Substituting Eq. (7) into Eq. (6) and taking the time-averaged, called Reynolds-averaged Navier-Stokes.

$$\rho\overline{u_j}\frac{\partial}{\partial x_j}(\overline{u_\iota}) = -\frac{\partial\bar{P}}{\partial x_i} + \frac{\partial}{\partial x_j}\left(2\mu\overline{S_{j\iota}} - \rho\overline{u_\iota' u_j'}\right) + \mathrm{F_i} \tag{9}$$

To calculate the Reynolds stresses, we employ the well-known Boussinesq relationship.

$$\rho\overline{u_\iota' u_j'} = \frac{2}{3}\mathrm{k}\delta_{ij} - \mu_t\left(\frac{\partial\overline{u_j}}{\partial x_i} + \frac{\partial\overline{u_\iota}}{\partial x_j}\right) \tag{10}$$

Where:
the Kronecker delta, $\delta_{ij} = 1$ if i = j and $\delta_{ij} = 0$
if $i \neq j$

4.3 Turbulence models (Stander $k-\epsilon$ model)

The standard $(k-\epsilon)$ model is a type of two-equation model that deals with two different transport equations. The following transport equations of k are used in the regular k-model.
the following transport equations are used for k;

$$\rho u_j\frac{\partial\mathrm{k}}{\partial x_j} = \frac{\partial\mathrm{k}}{\partial x_j}\left((\mu + \frac{\mu_t}{\sigma_k})\frac{\partial\mathrm{k}}{\partial x_j}\right) + 2\mu_t S_{ij}.S_{ij} - \rho\epsilon \tag{11}$$

and ϵ;

$$\rho u_j\frac{\partial\epsilon}{\partial x_j} = \frac{\partial\epsilon}{\partial x_j}\left((\mu + \frac{\mu_t}{\sigma_\epsilon})\frac{\partial\epsilon}{\partial x_j}\right) + C_{1\epsilon}\frac{\epsilon}{k}\mu_t S_{ij}.S_{ij} - C_{2\epsilon}\rho\frac{\epsilon^2}{\mathrm{k}} \tag{12}$$

The values for these constants were determined by fitting extensive data to the standard $k-\epsilon$ model. The values are [13]:

C_μ	σ_k	σ_ϵ	$C_{1\epsilon}$	$C_{2\epsilon}$
0.09	1.00	1.30	1.44	1.92

5 Theoretical Model

The total pressure drop of the perforated pipe can be calculated from.

$$\Delta P_T = \Delta P_f + \Delta P_{per} + \Delta P_{mix} + \Delta P_{acc.} \tag{13}$$

5.1 Friction Pressure Drop

This is caused by wall friction resulting from the sum of (wall friction pressure drop and perforations roughness). According to most researchers [3, 6, 8, 14]. For all types of fully developed flows in wellbore internal flows (laminar and turbulent flow) and rough or smooth surfaces, the pressure drop due to pipe wall friction is calculated using the Darcy Weisbach 1986 equation for all types of fully developed flows in wellbore internal flows (laminar and turbulent flow).

$$\Delta P_f = f_t \frac{L}{D} \frac{\rho u^2}{2} \quad (14)$$

f_t: represents the total friction factor for pipe (dimensionless).
L: total length of the pipe, D inner diameter of the pipe

The total friction factor quantifies the force produced by the fluid on the wall in a turbulent flow. The equation can be used to compute the friction factor.

$$f_t = f_o + \mathrm{f_p} \quad (15)$$

The friction factor in turbulent pipe flow is Haaland (1983) equation [15].

$$\frac{1}{\sqrt{f_0}} = -1.8 \log\left(\frac{6.91}{Re} + \left(\frac{\epsilon}{3.7D}\right)^{1.11}\right) \quad (16)$$

A mathematical model to calculate the friction factor is presented in [9], in which this gives

$$f_p = 4D\ \frac{q}{Q} + 2\frac{D}{n}(\frac{q}{Q})^2 \quad (17)$$

5.2 Acceleration Pressure Drop

The acceleration pressure drop is caused by axial velocity change (momentum change). It depends on the density of the liquid and the average velocity at the end of the outlet pipe.

$$\Delta P_{acc.} = \rho(u_{out}^2 - u_{in}^2) \quad (18)$$

Where u_{in} , u_{out} the average velocity of the fluid at inlet and outlet of the pipe, respectively.

5.3 Mixing Pressure Drop

Pressure drops owing to passage through perforations causing mixing. It is caused by the complicated interplay of perforation and wellbore flow, which causes disruptions in the boundary layer and hence impacts the pressure drop. When liquid fluid enters the wellbore through a perforation, it mixes with the mainstream and adds to the well's bulk. Su and Gudmundsson [16] created formulae that can be used to determine the mixing pressure drop when the flow rate is larger than 0.0025, this equation is applied.

$$\Delta P_{\mathrm{mix}} = 760\left(\frac{q}{Q}\right) \quad (19)$$

$\frac{q}{Q}$: The total flow rate ratio (q) is the total perforation flow rate divided by the total flow rate at the pipe outlet.

5.4 Productivity Index (PI)

The productivity index is defined based on the mathematical equation resulting from dividing the outflow from the main pipe on the total pressure drop.

$$PI = \frac{Q_3}{\Delta P_T} \quad (20)$$

5.5 Average wall shear stress

The distribution of wall shear stress is altered by changes in the velocity gradient at the wall. The velocity gradient at the wall and the local effective viscosity, which is the sum of molecular and turbulent viscosity, determine wall shear stress in turbulent flow [17].

$$\tau_W = (\mu + \mu t)\frac{du}{dy} \quad (21)$$

6 Grid Independence Test

To verify the results of the numerical solution using the ANSYS FLUENT program. The maximum mesh size is determined to obtain the correct values in the first phase of the numerical simulation. In this study, the mesh is constructed using a CFD tetrahedron with different maximum mesh sizes. The maximum mesh changing is used to show the best mesh properties that can be used for a simulation for all cases in this simulation. Three boundary layers are used on the wall of the pipe, representing the type of mesh methods in Fig.2, and represent the mesh properties in Table 2.

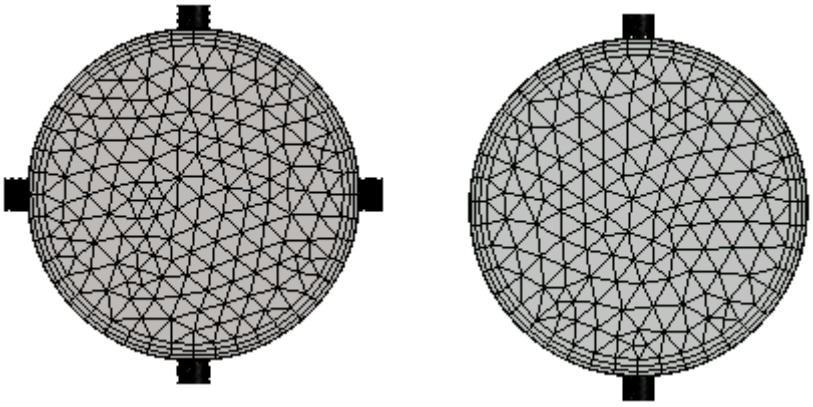

Fig. 2. Cross geometry of the test pipe in the 180° and 90° perforation phasing.

Table 2. Mesh properties.

Number of perforation	perforation Phasing	nodes	element	Mesh metric
19	180°	254372	974705	**Skewness**
20	90°	275394	1063960	**Skewness**

7 Model Validation

The numerical models for the validity of the solution must be validated by comparing the results acquired by other researchers. The validation is carried out by comparing the CFD FLUENT findings to the experimental results of Ref [7]. A partially perforated 3-D horizontal pipe length of 1300 mm and 22mm inner dim, perforation phasing of 60°, and a perforation density of 12 SPF. This validation's boundary conditions are as follows in Table 3.

Table 3. Details of the flow in Ref [7].

Test	Axial Flow (lit/hr)	Radial Flow (lit/hr)
Test 1	5618- 5157	**0 - 854**
Test 2	3836- 3361	**0- 841**

Fig. 3 shows the pressure drop of the present work and [7]. The figure explains that the maximum error is 14.2% for the first flow test at zero flow rate ratio and decrease to 4.4% at total flow rate ratio equal to 0.13391, for flow test 2 the maximum error is 14.8% at total flow rate ratio equal to zero and decrease to 4.5 % at total flow rate ratio equal to 0.1865. It also demonstrates that there is a difference across all tests. This is due to a different range of Reynolds number values and higher than experimental experiments. As well as the difference between the experimental values calculated from the device and the values calculated from the Ansys program.

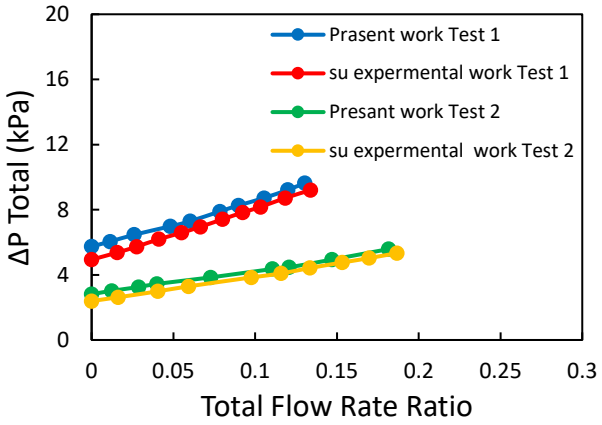

Fig. 3. Comparison of the present work with Ref [7].

8 Results and Discussion

A numerical study by using ANSYS Fluent and equations conducted on the perforated pipe at an angle of 180° and 90° to calculate pressure drop, friction, acceleration, and mixing. As well as, the study of the apparent friction factor, productivity index, velocity profile, and wall shear stress. The study is conducted for several flow rates as illustrated in Table 1.

8.1 Total Pressure Drop

Figs 4 and 5 represent the variations of pressure and flow rate ratio. It is shown that the total pressure drop increase as the flow rate ratio increase (an increase in radial flow for keeping the axial flow through the pipe constant). It is noticed this increase in the overall pressure drop is due to an increase in acceleration pressure drop. The tests line for the axial flow is 40, 60, 80,120, and 160 lit/min and constant radial flow from 0 - 80 lit/min. The Percentage error between 180° and 90° degrees for the five tests are 4.5%,3.2%,2.4%,4.2%, and 5.4%, respectively.

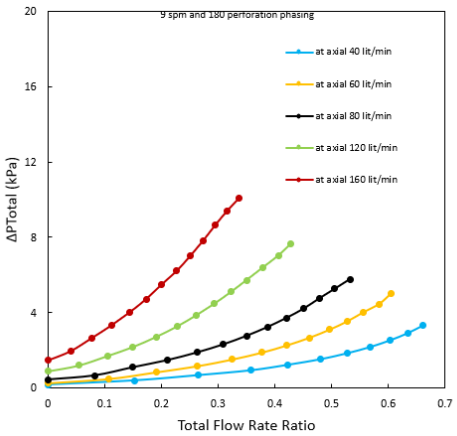

Fig.4. Total pressure drop in 180° perforation phasing

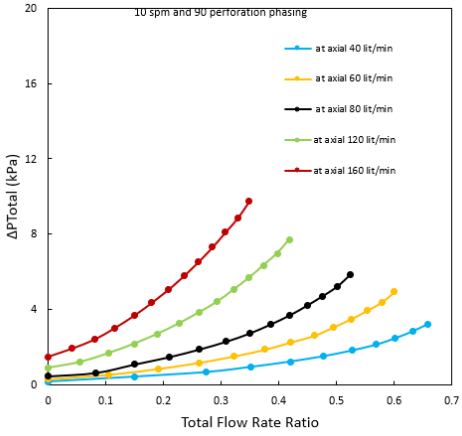

Fig. 5. Total pressure drop in 90° perforation phasing

8.2 Pressure Drop in Perforation Pipe

Figs 6 and 7 represent the variations of pressure drop and the total flow rate ratio. It is found that the total pressure drops increases with increasing the total flow rate ratio. This effect was caused by a larger decrease in wall frictional pressure as flow velocity increased. The proportion of the flow rate increases as the rate of the flow-through perforations increases, and increased the pressure drop. The main reason is that the perforations results in a greater decrease in the acceleration pressure caused by the flow through the perforations, thus increasing the mixing effect. It is observed that the acceleration values are lower in the wellbore pressure drop than the frictional pressure drops in resulting (wall friction and perforation roughness). For the results in the 180° perforations angle, the wall friction pressure reduced to 65.9% of the whole pressure rate, along with 31.6% acceleration pressure and 2.5% of mixing pressure. While for results in the 90° perforations phasing, the friction pressure drop is about 68.7%, and 28.5% acceleration pressure drop, and 2.8% drop of mixing pressure. The percentage error between 180° and 90° of test 5 is 5.4%.

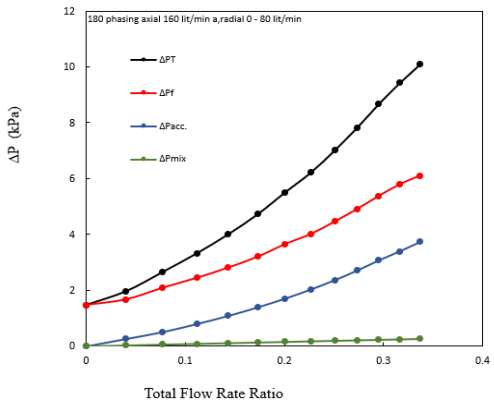

Fig. 6. Pressure Drop in 9 spm and 180° phasing

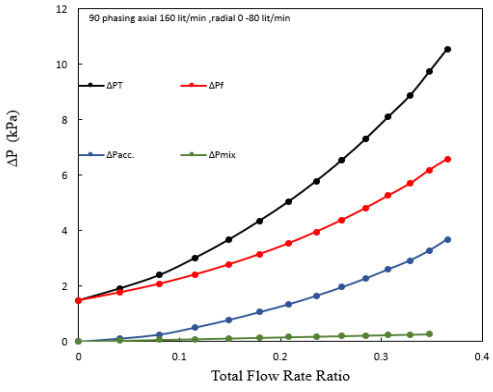

Fig. 7. Pressure Drop in 10 spm and 90° phasing

8.3 Static Pressure Drop

Figs.8 and 9 represent distribution pressure contour for the perforated pipe at 160 lit/min axial flow and 80 lit/min of radial flow. It is noticed from the results of the pressure decreases gradually, because of higher density and viscosity in this area. The maximum percentage error of pressure contour between 180° and 90° perforation phasing is 3.94%.

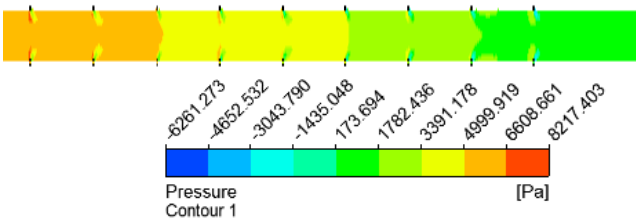

Fig. 8. Pressure at the perforated pipe in the 180° perforation phasing

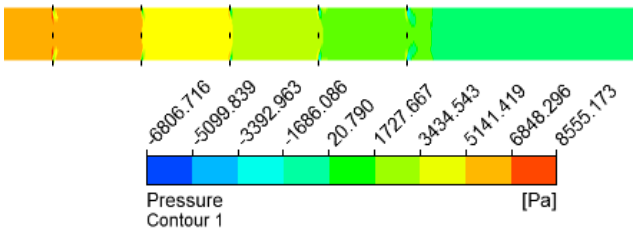

Fig 9. Pressure at the perforated pipe in the 90° perforation phasing.

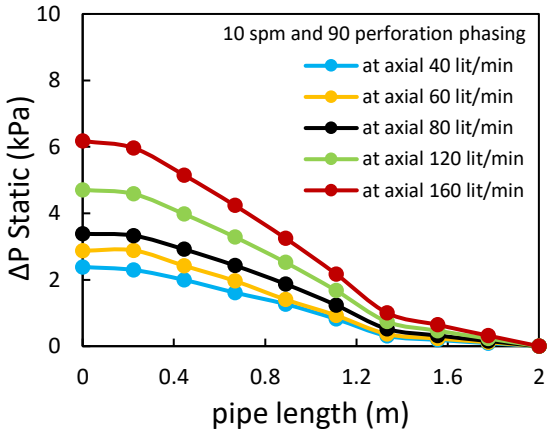

Fig. 10. Static pressure drops along the pipe length.

Figs10 and 11 represent the pressure drop along the centreline of the horizontal wellbore at various flow rates. The gradient has arrived at a fixed value as the pressure drop increased at the pipe's entry because entrance approximately 0.2 m downstream, and a sharp dropping of pressure at the horizontal pipe flow equalize the radial perforations flow. The static pressure at the pipe exit is going to be constant. When the axial-flow are 40,60,80,120,160 lit/min and the constant radial flow is 80 lit/min.

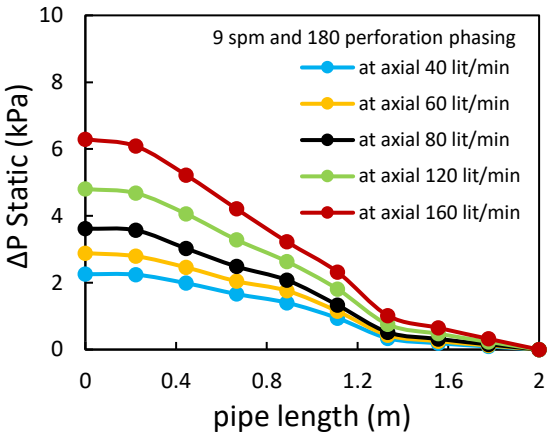

Fig 11. Static pressure drops along pipe length in the 180° perforation phasing in the 90° perforation phasing.

8.4 Friction Factor

Figs12 and 13 represent the relation between the total Friction factor and the total flow rate ratio. This is increased with increasing flow ratio rate, due to the change in the velocity field resulting from the flow through the perforations. The axial and radial flow rates were selected from Table 1.

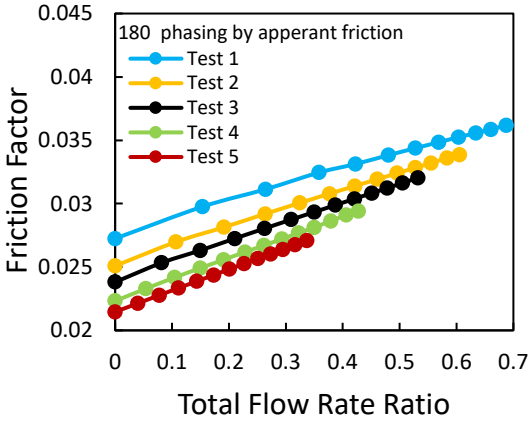

Fig.12. Total friction factor in the 180° phasing phasing

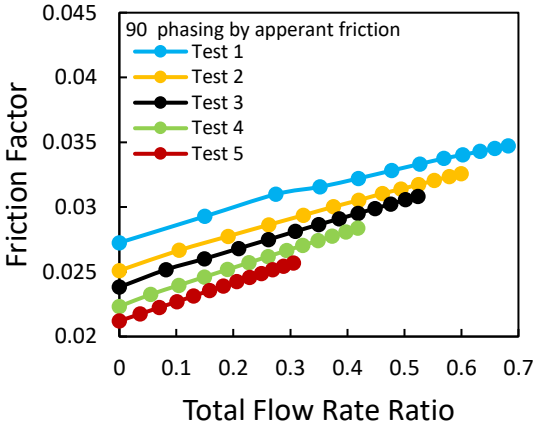

Fig.13. Total friction factor in the 90°

8.5 Productivity Index

Fig.14 and Fig. 15 represent the relationship of the productivity index with the total flow rate ratio. It is observed that the productivity index lowered with increasing the flow rate ratio, the reason for the decrease in the productivity index is due to the increases in the total pressure drop along the pipe. Also, the increase of the overall pressure drop is greater than the flow rate of the main pipe through the perforations, which leads to decreases in the productivity index. The axial and radial flow rates were selected from Table 1.

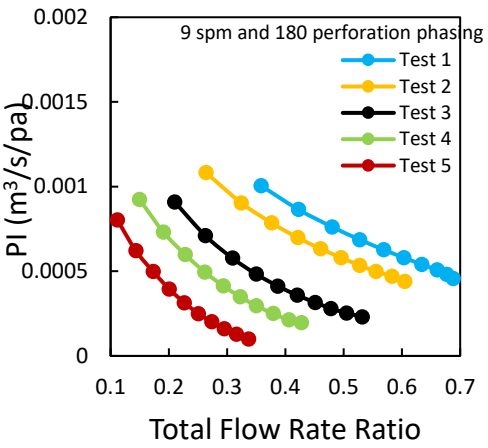

Fig. 14. Productivity index in the 180° phasing

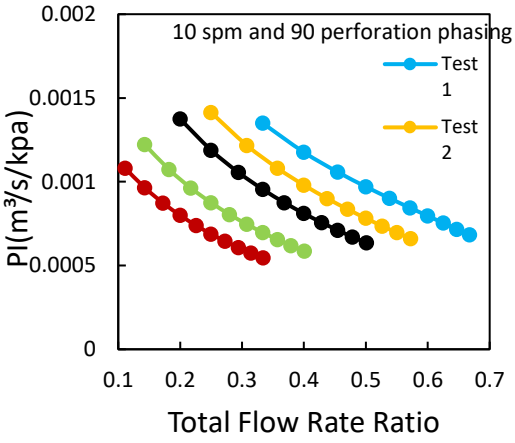

Fig. 15. Productivity index in the 90° phasing

8.6 Average velocity in the centre-line of perforation pipe

Figs16 and 17 represent the variations of velocity of planes along the pipe length. It is observed the flow in the perforation disrupts the axial flow in the pipe. and this increases the velocity in the wellbore pierced due to the radial flow entering through the perforation. Also, because of the reduction in the velocity of fluid flow near the wall. The test line for the flow of constant of radial flow 80 lit/min, and change of axial flow from range 40, 60,80,120,160 lit/min. It is noted from the figure that the distribution of the perforations has an angle of 90° better than 180°, and this leads to that the velocity out main of the pipe 90° is more stable than 180°.

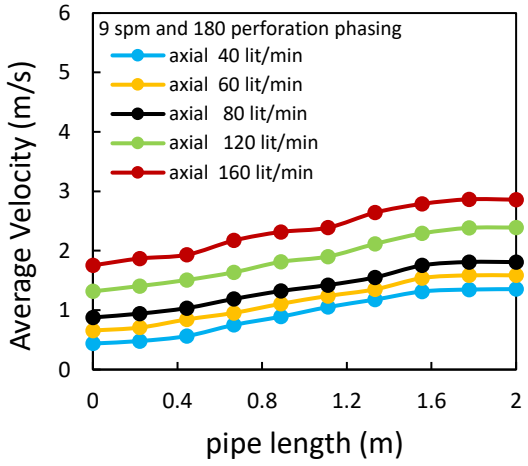

Fig 16. Average velocity along pipe length in the 180° perforation phasing

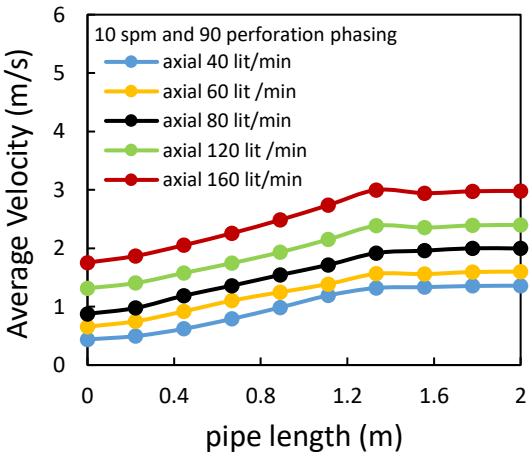

Fig 17. Average velocity along the pipe length in the 90° perforation phasing

Figs 18 and 19 represent the velocity distribution contour for the test pipe along the good pipe with flow 160 lit/min, and radial 80 lit/min. It is noticed that the axial/radial flow at the junction causes the flow velocity to increase in the perforation section of the pipe. It is observed that there is a pressure drop and rises the perforated rate.

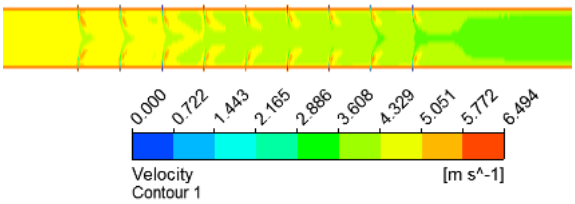

Fig.18. velocity contour in the 180° phasing

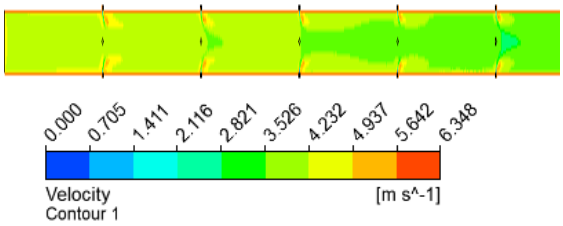

Fig 19. Velocity contour in the 90° phasing.

8.7 Velocity Profile

Figs 20 and 21 represent the velocity profiles in the direction of changing cross-section in exit perforation section for plane x=1.35 m for a perforated phasing 180° and 90° with at change the axial flow 40,60,80.120.160 lit/min and constant radial flow through the perforations of 80 lit/min. It is noted that axial flow rate increases with constant perforations, the change in velocity become higher with the direction of the change of cross-section.

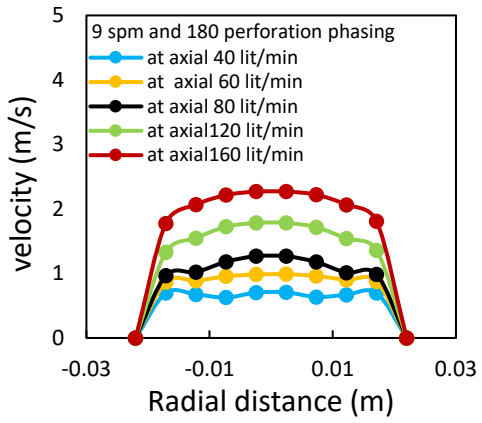

Fig 20. Distribution of velocity profile at the exit perforation section in the 90° perforation phasing

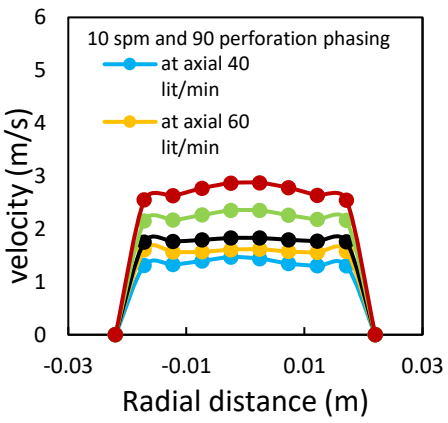

Fig 21. Distribution of velocity profile at the exit perforation section in the 180° perforation phasing

8.8 Average wall shear stress

The link between the average wall shear stress and the overall flow rate ratio is depicted in Figures 22 and 23. Because of the interplay between the axial flow and the inflow through the perforation, the average wall shear stress increases as the total flow rate ratio rises. As a result, inflow elevates and expands the turbulent boundary layer, increasing axial velocity beyond the layer while lowering velocity within it, as the mass conservation equation dictates.. The

maximum percentage error of average wall shear between 180° and 90° perforation phasing of test 5 is 10%.

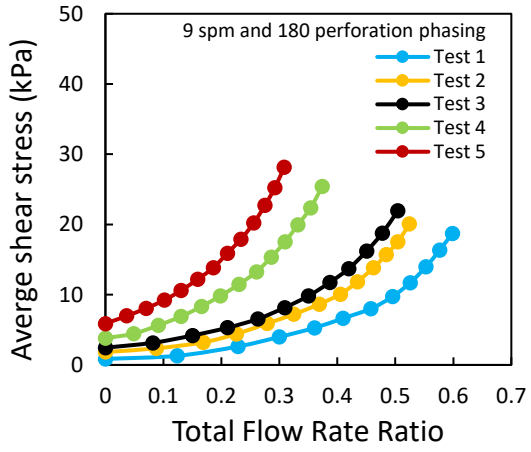

Fig. 22. Average well shear stress in the 180° perforation phasing

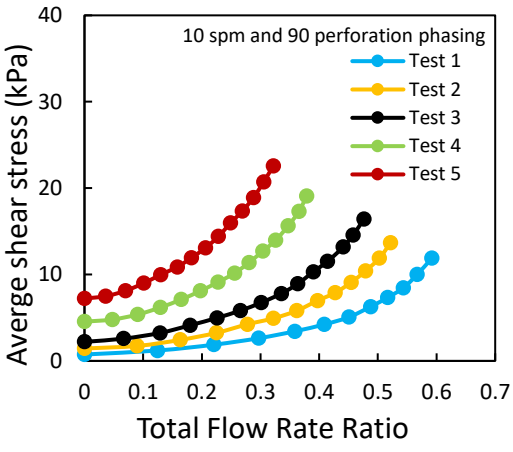

Fig. 23. Average well shear stress in the 90° perforation phasing

9 Conclusions

Numerical simulations of pipe flow, a numerical study has been conducted on the perforated pipe in 180°and 90° perforation angle of the flow horizontally wellbore. Simulation conducted using the ANSYS and stander $k-\varepsilon$ model. The study shows the following conclusions:

1- The total pressure reduced linearly with increasing the total flow rate ratio. The total pressure drop has the angle of the perforations 90° greater than the angle of the perforations 180° because the distribution of the perforations at the angle 90° is better than 180°

2-It is noticed that the greater the flow through perforations increase pressure drop and vice versa.

3- Field velocity at the entrance is completed as the flow increases up to the perforations. Axial direction collides with each other with radial flows, the fluid velocity in the downstream wellbore wall is less than the velocity from the inlet pipe wall to the upstream, but the velocity behaviour throughout the centre from the whole pipe does not change.

4- It is concluded that the flow rate increased, which leads total pressure drop and lower the productivity index. The productivity index of the angle perforation 90° is more productive than the perforation angle of 180°. Flow-through wellbore with an angle of 90 ° greater than 180 ° increases.

5- Increasing the flow rate through the perforations increases the wall shear stress.

References

[1] Stanley Locks., "An Advanced Method for Predicting the Productivity Ratio of a Perforated Well," Society of Petroleum Engineers of AIMf, (1981) ; SPE-8804-PA- 23: 2481-2488.

[2] Islam, M.R. and Chakma., "A Comprehensive Physical and numerical Modeling of a Horizontal Well," Annual Technical Conference and Exhibition of the SPE ; New Orleans, LA, September 23-26, (1990) ; SPE 20627.

[3] Folefac, J.S. Archer, and Issa. Chakma.," Effect of Pressure Drop Along Horizontal Wellbores on Well Performance," Offshore Europe Conference, held in Aberdeen , September 3-6- (1991); SPE 23094.

[4] Knut Seines, Ivar Aavatsmark, and S.C. Lien.," Considering Wellbore Friction Effects in Planning Horizontal Wells," Society of Petroleum Engineers of AIMf, October 1993; SPE-21124-PA.

[5] Cem Sarica, U. of Tulsa, Erdal Ozkan ,and Mustafa Haciislamoglu.," Influence of Wellbore Hydraulics on Pressure Behavior and Productivity of Horizontal Wells," Annual Technical Conference and Exhibition of the SPE; New Orleans, LA, September 25-28, (1994) ; SPE 28486 .

[6] Su, Z. and Gudmundsson, J.S., " Pressure Drop in Perforated Pipes," Asia Pacific oil & gas Conference held in Meibourna of the SPE; Australia, November 7-10- 1994 ; SPE 28800.

[7] Harald Asheim ,Johnny Kolnes ,and Piet Oudeman., "A Flow Resistance Correlation for Completed Wellbore," J. Petrol. Sci. Eng, February 10, (1992) ; pp. 97-104 .

[8] Novy, R.A., " Pressure Drops in Horizontal Wells: When Can They be Ignored," Society of Petroleum Engineers, February (1995) ; SPE-24941-PA .

[9] Wellington Campos, Rogério Campos,and Divonsir Lopes., " Frictional and Accelerating Pressure Drops Effects on Horizontal Oil Well Productivity Index," 18th International Congress of Mechanical Engineering, November 6-11, (2005).

[10] Zeboudj Faycal Fayal and Bahi Lakhdar., " Horizontal Well Performance Flow Simulation CFD-Application," pSPE Production and Operations Conference and Exhibition; Tunis, June (2010) ; SPE 133269.

[11] Mohammed Abdulwahid, Niranjan Injeti and Sadoun Dakhil.," Numerical Simulation of Flow through Wellbore for Horizontal Wells," Proceedings of the International Conference on Applied Mathematics and Computational Methods in Engineering., (2013) ; pp. 40-48.

[12] Thomas Vyzikas., " Application of numerical models and codes," MERiFIC University of Plymouth. Numerical Modelling. February (2014) ; pp. 57 – 83.

[13] Versteeg HK, Malalasekera W.," An Introduction to Computational Fluid Dynamics," Turbulence and its modelling. Prentice Hall, (2007) ; pp. 66 -78.

[14] Hua L, Yan L, Xiaodong P, Xindong L, Laichao .," Pressure Drop Calculation Models of Wellbore Fluid in Perforated Completion Horizontal Wells," IJHT, Vol. 34, No. 1, March, (2016); pp. 65-72

[15] Haaland S.E.," Simple and Explicit Formulas for the Friction Factor in Turbulent Pipe Flow," Journal of Fluids Engineering 10, Mar (1983) ; pp. 589-590.

[16] Su, Z. and Gudmundsson, J.S.," Perforation Inflow Reduces Frictional Pressure Loss in Horizontal Wellbores," J. Petrol. Sci. Eng. March (1998) ; pp. 223-232.

[17] White, F.M., " Viscous Fluid Flow," Second Edition, McGraw-Hill, Inc. 1991: pp. 104 - 212.